Angle-resolved Wigner time delay in atomic photoionization: The 4d subshell of free and confined Xe

A. Mandal,[1,*] P. C. Deshmukh,[2,3,†] A. S. Kheifets,[4,‡] V. K. Dolmatov,[5,§] and S. T. Manson[6,‖]

[1]*Department of Physics, Indian Institute of Technology Madras, Chennai, Tamil Nadu 600036, India*
[2]*Department of Physics, Indian Institute of Technology Tirupati, Tirupati, Andhra Pradesh 517506, India*
[3]*Department of Physics, Indian Institute of Science Education and Research Tirupati, Tirupati, Andhra Pradesh 517507, India*
[4]*Research School of Physics and Engineering, The Australian National University, Canberra ACT 0200, Australia*
[5]*Department of Physics and Earth Science, University of North Alabama, Florence, Alabama 35632, USA*
[6]*Department of Physics and Astronomy, Georgia State University, Atlanta, Georgia 30303, USA*

The angular dependence of photoemission time delay for the inner $nd_{3/2}$ and $nd_{5/2}$ subshells of free and confined Xe is studied in the dipole relativistic random phase approximation. A finite spherical annular well potential is used to model the confinement due to fullerene C_{60} cage. Near cancellations in a variety of the dipole amplitudes, Cooper-like minima, are found. The effects of confinement on the angular dependence, primarily confinement resonances, are demonstrated and detailed.

I. INTRODUCTION

With the advancements in the state-of-the-art of laser pulse production and manipulation, time domain studies have become of significant interest, as well as very challenging [1–11]. It is now possible to study the dynamics of electrons on the atomic time scale, i.e., the attosecond (as) scale. Photoionization time-delay studies of various systems have been carried out, such as of free atoms, surfaces, molecules, encaged atoms, etc. [11–16]. Most of the measurements are the pump-probe type where the measured time delay can be separated into the Wigner contribution [17–19], which is a property of the one-photon ionization of the target, and the measurement-induced [Coulomb laser coupling (CLC) or continuum-continuum (CC)] parts [14]. In this study, we concentrate upon the Wigner time delay, a concept that was developed for collisions but has seen wide application to photoionization in recent years [16]. The phase of the one-photon ionization transition matrix element and its variation with respect to the energy, angle, correlation in initial and final states, polarization, presence of other potentials, etc. result in various structures in Wigner time-delay spectra. Thus, studies of atomic and molecular photoionization have received significant attention from both experimentalists and theorists. One of the possible bridges between the behavior of free (gaseous) atoms and condensed matter is the study of the atomic characteristics in the environment of an additional potential; hence, the study of the behavior of an atom under confinement, which is a system intermediate between a free atom and condensed matter, is both interesting and important. In addition, trapped atoms are of interest owing to their potential applications, such as their use in building qubits for quantum computation [20].

Many aspects of atoms confined in fullerenes have been studied in the recent past [21–27]. The effect of fullerene confinement on the photoionization time delay was studied very recently; it was found that confinement-induced correlation influences the temporal evolution of the photoelectron from different hybridized states of Ar confined within C_{60} (Ar@C_{60}) [15]. Furthermore, it was found that confinement effects are more prominent in the photoionization time-delay spectrum compared to other observables such as the cross section [28]. Thus, since (i) the understanding of the effects of confinement is of significant basic and applied importance [21,22], (ii) photoionization time delay is rather sensitive to the effects of confinement and confinement resonances, and (iii) photoionization time delay is, in general, anisotropic with respect to the polarization of the photon owing to the interference of continuum waves of differing angular momenta [29,30], a detailed study in this arena is needed. In addition, an important feature of probing a system with photons (as opposed to, say, electrons or heavy ions) is that photons cause a much weaker perturbation of the system, thereby allowing the study of the properties of the target, unencumbered by the interaction process.

In the present work, the effect of confinement on the angular dependence of Wigner time delay upon photoionization of the 4d subshell of atomic xenon confined in C_{60} (Xe@C_{60}) is investigated using the relativistic-random-phase approximation (RRPA). Xe@C_{60} was chosen for this case study because it can be synthesized in sufficient quantities to allow experimental scrutiny [31].

This paper is organized as follows. In Sec. II, a brief theoretical formulation is given. In Sec. III the results for the angle and energy dependence of Wigner time delay for photoemission from inner $4d_{3/2}$ and $4d_{5/2}$ subshells of free and confined atomic Xe are presented, compared, and discussed. Conclusions are drawn and a summary is presented in Sec. IV.

II. THEORETICAL METHOD

A. Photoionization amplitude

We adopt the multichannel RRPA formalism of Refs. [32,33] and follow the method as discussed in Ref. [30].

*amankur@physics.iitm.ac.in
†pcd@iittp.ac.in
‡a.kheifets@anu.edu.au
§vkdolmatov@una.edu
‖smanson@gsu.edu

For completeness, some detail of the calculation is given. The amplitude for a transition from the ground state (u_i) to an excited state ($\omega_{i\pm}$), induced by a time-varying external field $v_+ e^{-i\omega t} + v_- e^{i\omega t}$ is given by

$$T = \sum_{i=1}^{N} \int d^3r (\omega_{i+}^\dagger \vec{\alpha} \cdot \vec{A} u_i + u_i^\dagger \vec{\alpha} \cdot \vec{A} \omega_{i-}). \quad (1)$$

Here, $\vec{A}$ is the vector potential, and the electromagnetic interaction is written in Coulomb gauge, expressed in terms of the Pauli spin matrices

$$\vec{\alpha} = \begin{pmatrix} 0 & \vec{\sigma} \\ \vec{\sigma} & 0 \end{pmatrix}.$$

In a one-electron approximation, the multipole transition amplitude reduces to

$$T_{JM}^{(\lambda)} = \int d^3r \, \omega_{i+}^\dagger \vec{\alpha} \cdot \vec{a}_{JM}^\lambda u_i. \quad (2)$$

Here the indices J and M are the photon angular momentum and its projection and $\lambda = 1$ or 0 for electric or magnetic multipoles, respectively. Specifically, for a one-electron transition from an initial state characterized by the quantum numbers ljm to a linear combination of final continuum states $\bar{l}\bar{j}\bar{m}$ with the photoelectron spin described by a two-component spinor χ_ν, $T_{JM}^{(\lambda)}$ takes the form

$$T_{JM}^{(\lambda)} = i\sqrt{\frac{2\pi^2}{Ep}} \sqrt{\frac{(2J+1)(J+1)}{J}} \frac{\omega^J}{(2J+1)!!}$$
$$\times \sum_{\bar{\kappa}\bar{m}} (\chi_\nu^\dagger \Omega_{\bar{\kappa}\bar{m}}(\hat{p}))(-1)^{\bar{j}-\bar{m}} \begin{pmatrix} \bar{j} & J & j \\ -\bar{m} & M & m \end{pmatrix}$$
$$\times i^{1-\bar{l}} e^{i\delta_{\bar{\kappa}}} \langle \bar{a} \| Q_J^{(\lambda)} \| a \rangle (-1)^{\bar{j}+j+J}. \quad (3)$$

Here E and $\hat{p}$ are the photoelectron energy and momentum direction, respectively, ω is the photon frequency, $\delta_{\bar{\kappa}}$ is the phase of the continuum wave (with respect to free waves) with $\bar{\kappa} = \mp(\bar{j} + \frac{1}{2})$ for $\bar{j} = (\bar{l} \pm \frac{1}{2})$, respectively. In addition, κ is used below as shorthand for l and j with $\bar{\kappa}$ used similarly for $\bar{l}$ and $\bar{j}$. The spherical spinor is defined as

$$\Omega_{\kappa m}(\hat{n}) = \sum_{\nu=\pm 1/2} C_{l,m-\nu,1/2\nu}^{jm} Y_{lm-\nu}(\hat{n}) \chi_\nu. \quad (4)$$

The corresponding Clebsch-Gordan coefficients, C, are tabulated in Ref. [34]. The reduced matrix element of the spherical tensor between the initial state $a = (n\kappa)$ and a final energy scale normalized state $\bar{a} = (E, \bar{\kappa})$ is written as

$$\langle \bar{a} \| Q_J^{(\lambda)} \| a \rangle = (-1)^{j+1/2} [\bar{j}][[j]] \begin{pmatrix} j & \bar{j} & J \\ -\frac{1}{2} & \frac{1}{2} & 0 \end{pmatrix}$$
$$\times \pi(\bar{l}, l, J-\lambda+1) R_J^{(\lambda)}(\bar{a}, a). \quad (5)$$

Here $\pi(\bar{l}, l, J-\lambda+1) = 1$ or 0 for $\bar{l}+l+J-\lambda+1$ even or odd, respectively, $[j] = (2j+1)^{\frac{1}{2}}$, and $R_J^{(\lambda)}(\bar{a}, a)$ is the radial integral. While Eq. (5) is derived for a single-electron transition, it also applies to closed-shell atomic systems. In order to include the RRPA correlations, the only change in Eq. (3) is to replace $\langle \bar{a} \| Q_J^{(\lambda)} \| a \rangle$ with $\langle \bar{a} \| Q_J^{(\lambda)} \| a \rangle_{RRPA}$.

Finally, as we will be dealing with electric dipole photoionizing transitions, we set $\lambda = 1$, $J = 1$ and choose $M = 0$, which corresponds to linear polarization in the z direction. In this case,

$$T_{10}^{1\pm} \equiv [T_{10}^{(1)}]_{\nu=\pm 1/2} = \sum_{\bar{\kappa}\bar{m}} C_{l,\bar{m}-\nu,1/2\nu}^{j\bar{m}} Y_{l\bar{m}-\nu}(\hat{p})$$
$$\times (-1)^{2\bar{j}+j+1-\bar{m}} \begin{pmatrix} \bar{j} & 1 & j \\ -\bar{m} & 0 & m \end{pmatrix} i^{1-\bar{l}} e^{i\delta_{\bar{\kappa}}} \langle \bar{a} \| Q_1^{(1)} \| a \rangle. \quad (6)$$

Here we dropped the common scaling factor for brevity. In the following, we use a shorthand for the reduced matrix element modified by the phase factors:

$$D_{lj\to\bar{l}\bar{j}} = i^{1-\bar{l}} e^{i\delta_{\bar{\kappa}}} \langle \bar{a} \| Q_J^{(\lambda)} \| a \rangle. \quad (7)$$

B. Formulation of the angular-dependent time delay

In recent work [30], the relativistic formalism was applied for outer np ($np_{1/2}$ and $np_{3/2}$) subshells of Ar, Kr, and Xe in the Cooper minima region in their spectra. Wigner time delay was computed for these cases along with an estimate of CLC in the hydrogenic approximation. Here we employ this technique to study the Wigner time delay for a higher angular momentum state ($nd_{3/2}$ and $nd_{5/2}$) for the free as well as confined atom. An electric dipole transition from a nd initial state leads to the following six ionization channels:

$$nd_{3/2} \to \epsilon p_{1/2}, \epsilon p_{3/2}, \epsilon f_{5/2}$$
$$nd_{5/2} \to \epsilon p_{3/2}, \epsilon f_{5/2}, \epsilon f_{7/2}.$$

Using Eq. (6), we derive the following expressions for the $nd_{3/2}$ ionization amplitudes:

$$[T_{10}^{'(1+)}]_{nd_{3/2},1/2} = -\frac{1}{3\sqrt{2}} D_{nd_{3/2}\to\epsilon p_{1/2}} Y_{10}(\hat{p})$$
$$+\frac{1}{3}\sqrt{\frac{2}{5}} D_{nd_{3/2}\to\epsilon p_{3/2}} Y_{10}(\hat{p})$$
$$+\sqrt{\frac{3}{70}} D_{nd_{3/2}\to\epsilon f_{5/2}} Y_{30}(\hat{p}); \quad (8)$$

$$[T_{10}^{'(1-)}]_{nd_{3/2},1/2} = \frac{1}{3} D_{nd_{3/2}\to\epsilon p_{1/2}} Y_{11}(\hat{p})$$
$$+\frac{1}{6\sqrt{5}} D_{nd_{3/2}\to\epsilon p_{3/2}} Y_{11}(\hat{p})$$
$$-\sqrt{\frac{2}{35}} D_{nd_{3/2}\to\epsilon f_{5/2}} Y_{31}(\hat{p}); \quad (9)$$

$$[T_{10}^{'(1+)}]_{nd_{3/2},3/2} = \frac{1}{2}\sqrt{\frac{3}{5}} D_{nd_{3/2}\to\epsilon p_{3/2}} Y_{11}(\hat{p})$$
$$+\sqrt{\frac{2}{105}} D_{nd_{3/2}\to\epsilon f_{5/2}} Y_{31}(\hat{p}); \quad (10)$$

$$[T_{10}^{'(1-)}]_{nd_{3/2},3/2} = -\sqrt{\frac{1}{21}} D_{nd_{3/2}\to\epsilon f_{5/2}} Y_{32}(\hat{p}). \quad (11)$$

The angular-resolved amplitudes for the $nd_{5/2}$ initial state take the following forms:

$$\left[T_{10}^{'(1+)}\right]_{nd_{5/2,1/2}} = \frac{1}{\sqrt{15}}D_{nd_{5/2}\rightarrow\epsilon p_{3/2}}Y_{10}(\hat{p})$$

$$-\frac{1}{7\sqrt{10}}D_{nd_{5/2}\rightarrow\epsilon f_{5/2}}Y_{30}(\hat{p})$$

$$-\frac{\sqrt{2}}{7}D_{nd_{5/2}\rightarrow\epsilon f_{7/2}}Y_{30}(\hat{p}); \quad (12)$$

$$\left[T_{10}^{'(1-)}\right]_{nd_{5/2,1/2}} = \frac{1}{\sqrt{30}}D_{nd_{5/2}\rightarrow\epsilon p_{3/2}}Y_{11}(\hat{p})$$

$$+\frac{1}{7}\sqrt{\frac{2}{15}}D_{nd_{5/2}\rightarrow\epsilon f_{5/2}}Y_{31}(\hat{p})$$

$$-\frac{1}{7}\sqrt{\frac{3}{2}}D_{nd_{5/2}\rightarrow\epsilon f_{7/2}}Y_{31}(\hat{p}); \quad (13)$$

$$\left[T_{10}^{'(1+)}\right]_{nd_{5/2,3/2}} = \frac{1}{\sqrt{15}}D_{nd_{5/2}\rightarrow\epsilon p_{3/2}}Y_{11}(\hat{p})$$

$$-\frac{1}{7}\sqrt{\frac{3}{5}}D_{nd_{5/2}\rightarrow\epsilon f_{5/2}}Y_{31}(\hat{p})$$

$$-\frac{5}{14\sqrt{3}}D_{nd_{5/2}\rightarrow\epsilon f_{7/2}}Y_{31}(\hat{p}); \quad (14)$$

$$\left[T_{10}^{'(1-)}\right]_{nd_{5/2,3/2}} = \frac{1}{7}\sqrt{\frac{3}{2}}D_{nd_{5/2}\rightarrow\epsilon f_{5/2}}Y_{32}(\hat{p})$$

$$-\frac{1}{14}\sqrt{\frac{10}{3}}D_{nd_{5/2}\rightarrow\epsilon f_{7/2}}Y_{32}(\hat{p}); \quad (15)$$

$$\left[T_{10}^{'(1+)}\right]_{nd_{5/2,5/2}} = -\frac{1}{7}\sqrt{\frac{5}{6}}D_{nd_{5/2}\rightarrow\epsilon f_{5/2}}Y_{32}(\hat{p})$$

$$-\frac{\sqrt{6}}{14}D_{nd_{5/2}\rightarrow\epsilon f_{7/2}}Y_{32}(\hat{p}); \quad (16)$$

$$\left[T_{10}^{'(1-)}\right]_{nd_{5/2,5/2}} = \frac{\sqrt{5}}{7}D_{nd_{5/2}\rightarrow\epsilon f_{5/2}}Y_{33}(\hat{p})$$

$$-\frac{1}{14}D_{nd_{5/2}\rightarrow\epsilon f_{7/2}}Y_{33}(\hat{p}). \quad (17)$$

The corresponding amplitudes with negative m projection have exactly the same structure, owing to the symmetry about the photon polarization (z-direction) axis, so they are not given explicitly. Each nd_j amplitude has its own photoelectron group time delay (Wigner time delay) [17,18]) defined as (in atomic units)

$$\tau = \frac{d\eta}{dE}, \eta = \tan^{-1}\left[\frac{\mathrm{Im}T_{10}^{1\pm}}{\mathrm{Re}T_{10}^{1\pm}}\right]. \quad (18)$$

For the situation where neither the orientation of the residual ion nor the spin of the photoelectron is detected, the angle-dependent time delay is evaluated as

$$\tau_{nd_j}(\theta) = \frac{\sum_{m,\nu}\tau_{nd_{j,m,\nu}}(\theta)\left|\left[T_{10}^{'(1\nu)}\right]_{nd_{j,m}}\right|^2}{\sum_{m,\nu}\left|\left[T_{10}^{'(1\nu)}\right]_{nd_{j,m}}\right|^2}, \quad (19)$$

which is the weighted average of the initial m states and final spin states of the photoelectron. Note, incidently, that the situation is somewhat more complicated for circularly

polarized incident photons where the amplitudes for positive and negative m differ.

III. RESULTS AND DISCUSSION

Since photoionization of atoms involves correlated many-electron dynamics, the *ab initio* relativistic random-phase approximation (RRPA), which includes both relativistic interactions (since it is based on the Dirac equation) and many-electron correlation effects [32,33], is applied for the calculation of the dipole matrix elements and transition amplitudes. In order to include final-state correlations (interchannel coupling), the calculations have been performed with the following 13 coupled channels:

$$5p_{3/2} \rightarrow \epsilon d_{5/2}, \epsilon d_{3/2}, \epsilon s_{1/2},$$

$$5p_{1/2} \rightarrow \epsilon d_{3/2}, \epsilon s_{1/2},$$

$$5s_{1/2} \rightarrow \epsilon p_{3/2}, \epsilon p_{1/2},$$

$$4d_{5/2} \rightarrow \epsilon f_{7/2}, \epsilon f_{5/2}, \epsilon p_{3/2},$$

$$4d_{3/2} \rightarrow \epsilon f_{5/2}, \epsilon p_{3/2}, \epsilon p_{1/2}.$$

The calculations have been carried out from about 15 eV above the $4d$ thresholds up to a photon energy of 150 eV; the near-threshold region, where the Wigner time delay is dominated by the Coulomb phase, is not considered. The omission of the photoionization channels from more tightly bound subshells, starting with $4p$ and on down, is unimportant since they contribute only a negligible amount to the $4d$ matrix elements in the chosen range of energies. Note that earlier calculations based upon the RRPA formalism have been found to be in very good agreement with experiment in many previous studies (see, for example, Refs. [28,35,36] and references therein).

The effects of the fullerene C_{60} molecular cage was taken as a spherically attractive potential [$V(r)$] defined as

$$V(r) = \begin{cases} -V_0, & \text{for } r_0 \leqslant r \leqslant r_0 + \Delta; \\ 0, & \text{otherwise}, \end{cases}$$

[21] with inner radius (r_0) = 5.8 a.u., thickness (Δ) = 1.9 a.u., depth (V_0) = 0.302 a.u.. This model has been shown to be a reasonable approximation in a number of previous studies [21,31,37–40].

Since the RRPA methodology employs Dirac-Hartree-Fock (DHF) thresholds in the calculation, these threshold energies for the valence ($n = 5$) and inner ($n = 4$) subshells are shown in Table I for both free and confined Xe. Of note here is that the binding energies for the confined case are slightly larger for Xe@C_{60}, and that the differences get somewhat larger as the subshell depth increases. This occurs because a spherical shell potential shifts the potential for electrons fully inside the shell by a constant amount. However, if part of the charge density of a subshell is not contained fully inside the shell potential, the change is less; this has been pointed out and explained earlier in the context of alkali-earth atoms [41]. In any case, this is exactly what Table I reveals.

The Wigner time delays are calculated from the basic matrix elements for each amplitude as given in Eqs. (8)–(17). They are measurable, and we start with the time delay associated

TABLE I. Dirac-Hartree-Fock (DHF) thresholds for free and confined Xe in eV.

Subshell	Xe	Xe@C_{60}
$5p_{\frac{3}{2}}$	11.97	12.31
$5p_{\frac{1}{2}}$	13.40	13.78
$5s_{\frac{1}{2}}$	27.49	27.88
$4d_{\frac{5}{2}}$	71.67	72.21
$4d_{\frac{3}{2}}$	73.78	74.32
$4p_{\frac{3}{2}}$	162.80	163.34
$4p_{\frac{1}{2}}$	175.58	176.12
$4s_{\frac{1}{2}}$	229.38	229.93

with each of these amplitudes because the physics is most easily revealed in these individual, unaveraged, channels.

Shown in Fig. 1 are the Wigner time-delay results for the photoionization $4d_{3/2}$ in both free Xe and Xe@C_{60}. A ubiquitous feature of the results is the existence of confinement oscillations [42], which are present in all cases for the confined Xe atom; these are due to the interference of electron waves which are emitted directly, and the waves which are reflected back from the confining potential. It is seen that, with increasing photon energy, all time delays at all angles tend towards zero. This is a general phenomenon, seen previously [43]. It occurs because the phases of the various dipole matrix elements all tend to zero, with increasing energy [44]. In addition, for each amplitude that includes contributions from transitions to final states with different final angular momenta (hence spherical harmonics of different l), it is seen that the time delay is angular dependent. This occurs for three of the four amplitudes depicted in Fig. 1.

Scrutinizing now the time delays for each of the four $4d_{3/2}$ amplitudes individually, starting with the $4d_{3/2,1/2}^{+}$, the results are depicted on the top panel of Fig. 1. As can be seen from Eq. (8), the amplitude contains a linear combination of the spherical harmonics Y_{30} and Y_{10}, so that the time delay has an angular dependence, as seen in Fig. 1. However, in the chosen energy range, $D_{4d_{3/2} \rightarrow \epsilon f_{5/2}}$ is much larger than the $4d \rightarrow \epsilon p$ matrix elements so that the angular variation is fairly small at most energies; this is also seen in Fig. 1, except in the region of 90 eV. The nonmonotonic bump in the 30° time delay, as a function of energy, is owing to a combination of factors. First, 30° is near the kinematic node of Y_{30} (which is at about 40°). Since Y_{30} is the angular factor of the $D_{4d_{3/2} \rightarrow \epsilon f_{5/2}}$ term in Eq. (8), the terms in Eq. (8) become competitive at 30°, in contrast to other angles, causing considerable cancellation. Specifically, the interference causes an inflection point in the phase, in the 90 eV region, thereby resulting in the bump in the energy derivative of the phase. The situation for the confined case is essentially the same with the exception of the confinement oscillations; these are seen to be present at all angles.

For the $4d_{3/2,1/2}^{-}$ amplitude (see Fig. 1), the time-delay situation is somewhat similar with an angular dependence resulting from the interference of Y_{31} and Y_{11}, Eq. (9). In this case, however, Y_{31} has a node at about 63°. Correspondingly at 60° the contribution of the normally dominant $D_{4d_{3/2} \rightarrow \epsilon f_{5/2}}$ term in Eq. (9) is decreased considerably so that there is
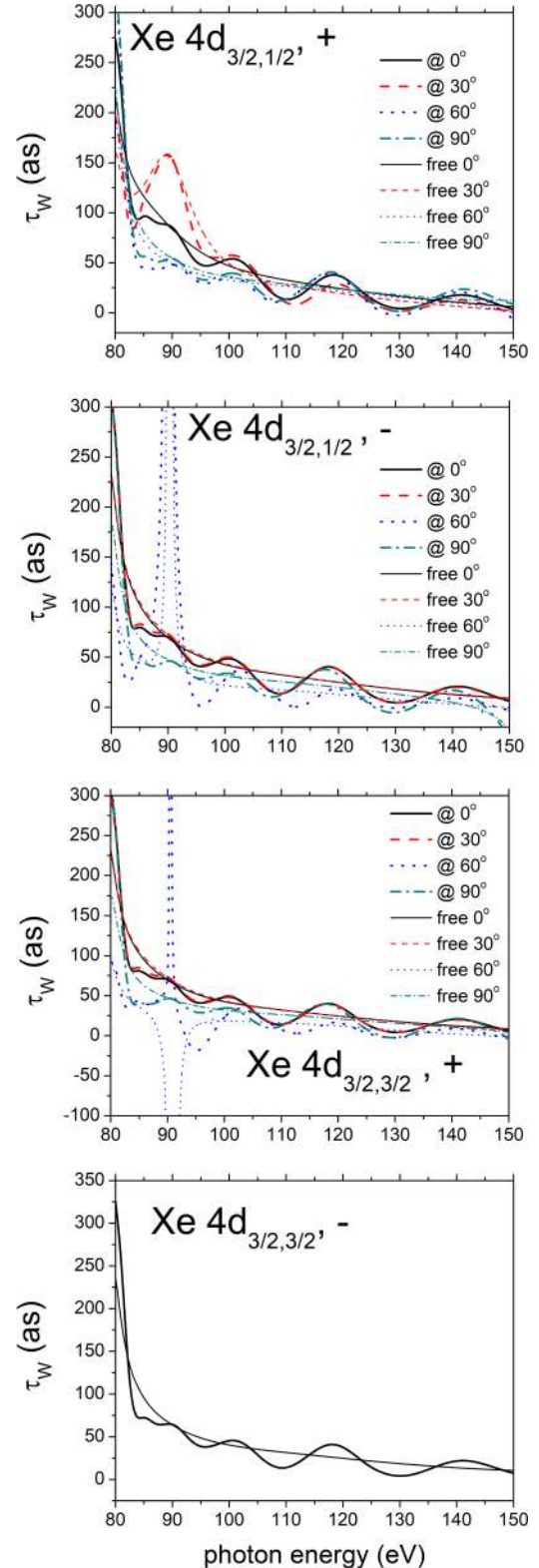

FIG. 1. Channel-specific time delay as calculated using Eqs. (8)–(11) for the $4d_{3/2}$ initial state. Bold lines are the Wigner time delay for Xe@C_{60} (abbreviated by @ in the figures) and thin lines are for free Xe. Different colors correspond to different angles.

significant interference among the terms. This results in a near cancellation around 90 eV, causing a Cooper-like minimum in the amplitude; the amplitude goes through a deep minimum

because both the real part and the imaginary parts go through zeros, but not exactly at the same energy, as in the case of an ordinary Cooper minimum. Thus, in that region, there is a very rapid increase in phase, followed by a very rapid drop, again just like in an ordinary Cooper minimum; there is a phase increase by π over a small energy region resulting in a huge spike in the time delay. This occurs in both the free and confined case, as seen in Fig. 1, i.e., the perturbating potential does not alter this cancellation. Additionally, as in the previous case, the confinement oscillations are present at all angles.

The $4d^+_{3/2,3/2}$ amplitude, shown in Fig. 1, is almost exactly like the previous case, except for the situation at 60° around 90 eV. The cancellation is much more tenuous in this case and the confinement has an important effect, as seen. The time delay for the free atom at 60° exhibits a deep dip rather than a rise. This occurs because near the Cooper-like minimum in the amplitude, where the imaginary part goes through a zero, the real part of the amplitude has the opposite sign compared to the other cases, thereby moving the phase in the opposite direction. The perturbing potential alters this, so that in the confined case, there is a spike, like the previous case, rather than a dip. Thus, there is a remarkable sensitivity of both the phase and the time delay, in the vicinity of these Cooper-like minima, to the details of the variations in the signs of the real and imaginary parts of the amplitude; this can be altered very significantly by a small perturbing potential. As a consequence, the difference in time delay at 60° in the 90 eV photon energy region between the free and confined atom is huge (by attosecond standards), of the order of femtoseconds.

For the $4d^-_{3/2,3/2}$ amplitude, also depicted in Fig. 1, there is only a single term in the amplitude, Eq. (11); hence, there is no angular dependence in this case. Thus, the time delay is isotropic. Correspondingly, the time delay is the result of the phase of the $D_{4d_{3/2}\to\epsilon f_{5/2}}$ transition, which is monotone decreasing for the free-atom case and yields a monotone decreasing time delay; the confined case is essentially the same except for the confinement modulations around the free-atom time delay.

The situation is similar for the time delays associated with the six $4d_{5/2}$ amplitudes, shown in Figs. 2 and 3, but with important differences that arise mainly because there is a significant interchannel coupling effect on the $4d_{5/2}$ photoionization matrix elements owing to the interaction with the $4d_{3/2}$ matrix elements known as spin-orbit-activated interchannel coupling (SOAIC), an effect than has been seen experimentally and interpreted theoretically in studies of photoionization cross sections [45,46]. Aside from the effect of interchannel coupling on the magnitude of the $4d_{5/2}$ matrix elements, whence the SOAIC effect arises, the coupling also affects the phase of the $4d_{5/2}$ matrix elements [47]. As a result, for example, the $4d_{5/2}$ cases show an inflection point in the phases in the 80 eV region. As a result, the time delay, the derivative of the phase, is small around 80 eV but rises with energy as the slope of the phase increases; it starts to drop off at somewhat higher energies, mimicking the $4d_{3/2}$ cases. In fact, except for the rise in time delay around 80 eV, the $4d^+_{5/2,1/2}$ result is rather similar to the $4d^+_{3/2,1/2}$ situation. This is not surprising since the structure of the expressions for the two amplitudes is quite similar. The confined case shows the same characteristics with the added confinement oscillations.
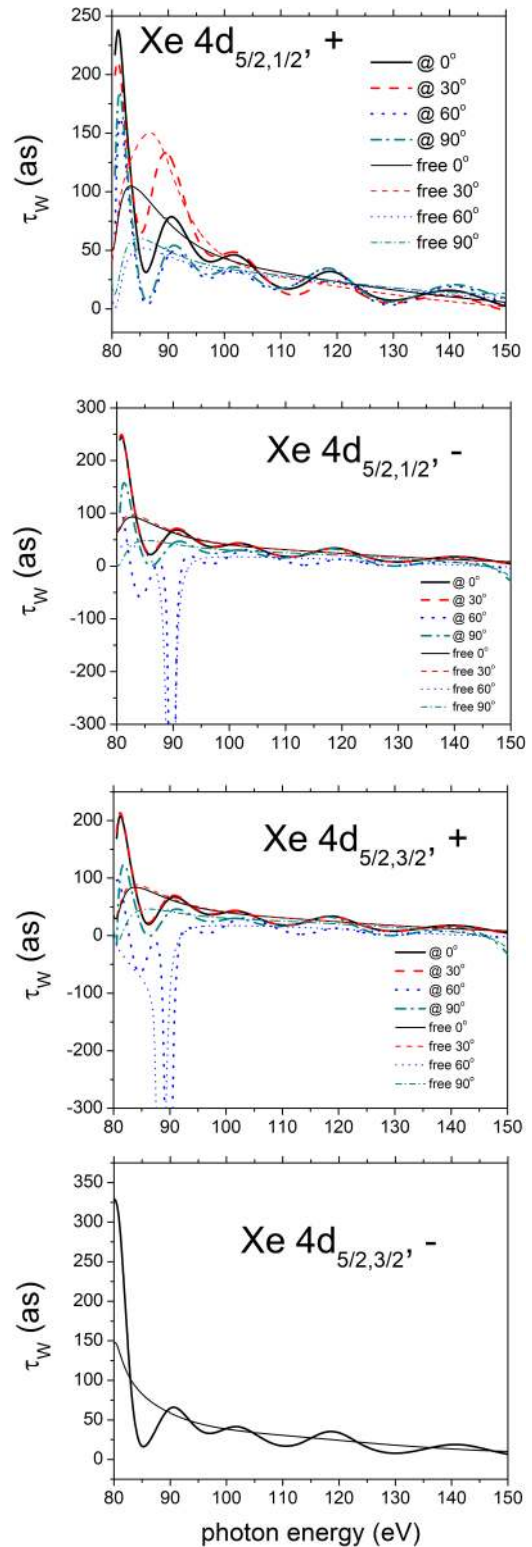

FIG. 2. Channel-specific time delay as calculated using (12)–(15) for $4d_{5/2}$. Bold lines are the Wigner time delay for Xe@C_{60} (abbreviated by @ in the figures) and thin lines are for free Xe. Different colors correspond to different angles.

Note that the structure of the amplitudes with the same initial state m quantum number and final-state photoelectron polarization ν are similar for both $4d_{3/2}$ and $4d_{5/2}$ initial
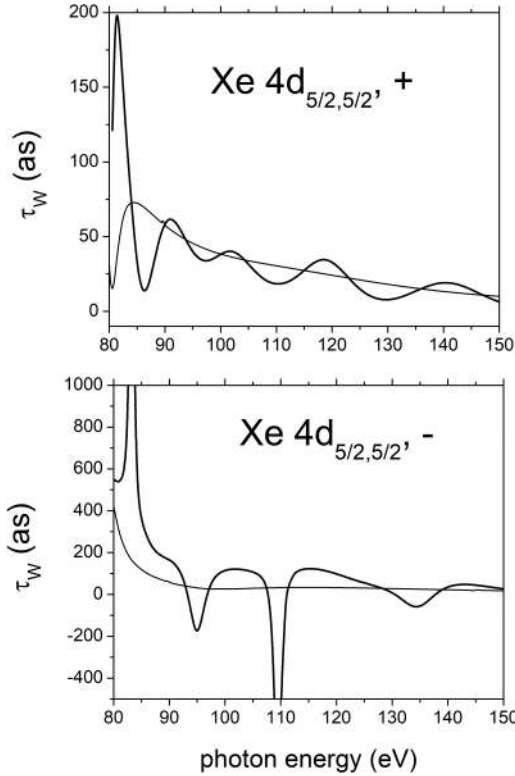
FIG. 3. Channel-specific time delay as calculated using (16)–(17) for $4d_{5/2}$. Bold lines are the Wigner time delay for Xe@C_{60} and thin lines are for free Xe.

FIG. 4. m and final-state spin average time delay for $4d_{3/2}$ and $4d_{5/2}$ as calculated using Eq. (19). Bold lines are the Wigner time delay for Xe@C_{60} (abbreviated by @ in the figures) and thin lines are for free Xe. Different colors correspond to different angles.

states, not only in the above case, but in all cases. Thus, it is evident that the time delays should be similar as well. This is exactly what is seen from the comparison of Fig. 1 and Fig. 2, with some differences owing to relativistic dynamics. One difference is the rising of the $4d_{5/2}$ time delays at around 80 eV for most cases, owing to the interchannel coupling, as explained above. For another, unlike the $4d_{3/2,3/2}^{+}$ case, for $4d_{5/2,3/2}^{+}$ both the free and confined time delays show a large dip at $60°$ in the 90 eV region. The introduction of the confinement potential does not change the situation qualitatively for the $4d_{5/2,3/2}^{+}$ amplitude, although it is seen that it does move the dip up by a few eV to higher energy. Still another difference is seen in Fig. 2 for the $4d_{5/2,3/2}^{-}$ time delay as compared to $4d_{3/2,3/2}^{-}$. The sharp positive spike in the $4d_{3/2}$ case at $60°$ near 90 eV becomes a negative spike for $4d_{5/2}$. It is thus found that the Cooper-like minimum in the amplitudes have significant effects upon the time delay. It is also evident from the comparisons of the $4d_{3/2}$ and $4d_{5/2}$ initial states that relativistic effects can have huge consequences, particularly near these Cooper-like minima.

The $4d_{5/2,5/2}^{\pm}$ cases, Fig. 3, have no analog in the $4d_{3/2}$ manifold because the latter cannot have $m = 5/2$. Furthermore, since the present calculation is for linear polarization of the incident photons, the final continuum states for transitions from the $4d_{5/2,5/2}$ initial states must also have $m = 5/2$. This means that only transitions to $\epsilon f_{5/2,5/2}$ and $\epsilon f_{7/2,5/2}$ are possible (there can be no $4d \rightarrow \epsilon p$ transitions). This follows from Eqs. (16) and (17). In addition, since each amplitude involves
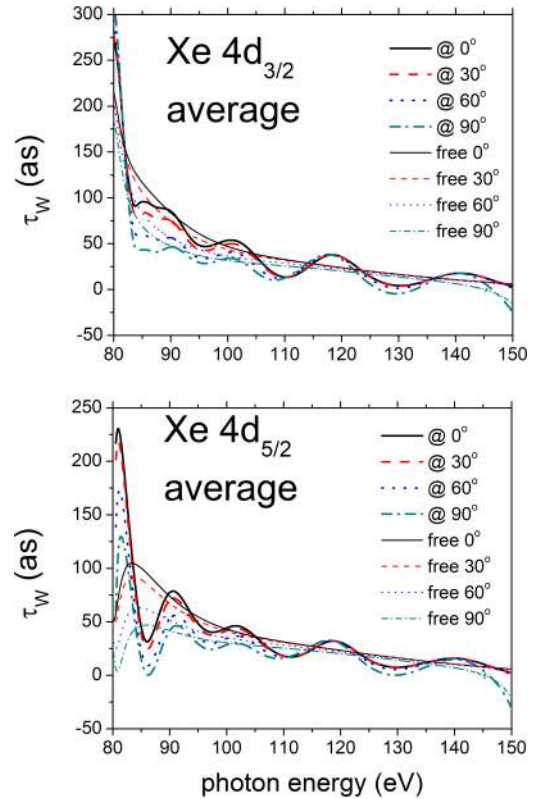
only a single spherical harmonic, the angular distribution must be isotropic; this is seen for both $4d_{5/2,5/2}^{\pm}$ cases in Fig. 3. Nevertheless, owing to relativistic interactions, each amplitude consists of two terms, which are slightly different and can interfere. The $4d_{5/2,5/2}^{+}$ case does not appear to show any significant effects of interference, although the confining potential induces a factor of five increase in the time delay at about 82 eV, thereby indicating the sensitivity of the time delay to small perturbations. For the $4d_{5/2,5/2}^{-}$ case, the free-atom time delay is monotone decreasing from 80 eV, which suggests that interference is going on in that energy region. The confined-atom time delay, however, is seen to behave quite differently; there is a very large positive spike at 85 eV and an equally large negative spike at about 110 eV. This occurs because the $4d_{5/2,5/2}^{-}$ amplitude is quite small since it is the difference of two roughly equal terms [Eq. (17)]. Thus, the addition of the confinement potential causes oscillations in the matrix elements. This results in not one but two Cooper-like minima in the amplitude, one around 80 eV and the other about 110 eV, resulting in the spikes. This does not happen in the $4d_{5/2,5/2}^{+}$ case because, as seen from Eq. (16), this amplitude is the sum of the two terms. It is noteworthy that the Cooper-like minima in the confined $4d_{5/2,5/2}^{-}$ case occur despite the absence of $4d \rightarrow \epsilon p$ transitions in this amplitude; this speaks to the importance of relativistic effects.

The calculated time delays for the weighted average over the initial-state magnetic quantum number m and the final-state photoelectron polarization [Eq. (19)] are depicted in Fig. 4. Of

importance here is that for free Xe, for the $4d_{3/2}$ initial state, the time delays are monotone decreasing with energy at all angles, while for the $4d_{5/2}$ initial state, they are rising from 80 eV (at all angles) and only start decreasing at higher energies. This occurs owing to the interchannel coupling between the $4d_{3/2}$ channels and the $4d_{5/2}$ channels, a purely relativistic effect, as explained in connection with the individual amplitude time delays. For the confined atoms, there are significant oscillations around the free results due to the confinement resonances. The amplitudes of these oscillations decrease with increasing energy, a well-known characteristic of confinement resonances [42]. It is also evident that these weighted averages do not exhibit any of the huge spikes, positive or negative, present in the time delays associated with the individual amplitudes. This happens because these spikes are typically related to the Cooper-like minima in the individual amplitudes so that, like ordinary Cooper minima, the cross sections are small in these regions and the effects are washed out in the weighted averages. It should be mentioned, however, that there are intermediate weighted averages that could be taken between the individual amplitude time delays and the Eq. (19) averages. One might consider the time delays in coincidence with photoelectron polarization. Then the average, Eq. (19), would be summed only over m, or in coincidence with the alignment of the residual ion, in which case the sum would be only over photoelectron polarization.

An important point to be emphasized, as mentioned earlier, is that pump-probe photoionization experiments involve the absorption of a second photon (streaking [7], RABBITT [9]). The presence of a second photon has consequences for the time delay. In fact, the measured time delay can be thought of as a sum of the Wigner time delay, τ_W, and $\tau_{CC/CLC}$, the time delay due to the second (probe) photon, also called Coulomb-laser coupling (CLC) [14] or continuum-continuum coupling (CC) [48].

$$\tau_{\text{atomic}} = \tau_W + \tau_{CC/CLC}. \tag{20}$$

The present calculation deals only with the Wigner time delay, τ_W. However, since the existing experimental techniques involve two photons, it is of interest to briefly discuss the consequences of the probe photon. $\tau_{CC/CLC}$ decreases rapidly from above the ionization threshold [49] and, thus, since the present calculations are well above the $4d$ thresholds, it is expected that it is small. The initial indication was that $\tau_{CC/CLC}$ is hardly dependent on the partial waves [49]. However, a recent RABBITT study of the angular-dependent time delay in He [50] showed this is not the case. The time delay from the spherically symmetric $1s$ shell becomes angular dependent close to the kinematic node of Y_{20} at the magic angle because of an enhanced competition of the $s \rightarrow p \rightarrow d$ and $s \rightarrow p \rightarrow s$ photoabsorption channel. This angular dependence of CLC corrections was also implicitly demonstrated in a recent theoretical study of the two-photon ionization of the $2p$ shell of Ne [51]. The Wigner time delay, taken alone, could not account for the calculated atomic time delay. Similarly, the second photon absorption can alter the presently calculated angular-dependent time delays. However, if the difference between the photoionization time delays for Xe and Xe@C_{60} are studied, $\tau_{CC/CLC}$, which depends upon the effective charge of the residual ion [14,48], should vanish

so that the measurement would return the difference in the free and confined Wigner time delays. It is hoped, therefore, that the present results might stimulate such a measurement.

IV. CONCLUSIONS

Wigner time delay in photoionization from $4d_{3/2}$ and $4d_{5/2}$ subshells has been calculated for free and confined Xe using a relativistic many-body formalism, the relativistic-random-phase approximation (RRPA). There were seen to be ten relativistic amplitudes from the $4d_{jm}$ initial states with positive values of m. It was found that six of the amplitudes generate a phase that is angle dependent, and thus, a Wigner time delay that depends upon the angle between the observation direction and the photon polarization direction. Over most of the energies and angles studied, the confined results were found to modulate around the free results with rather substantial amplitudes, tens of attoseconds or more, particularly at the lower energies, owing to the well-known confinement resonances. New effects were uncovered in the angular dependence of the Wigner time delay including Cooper-like minima in the amplitudes. In the vicinity of these Cooper-like minima, it was found that the phase of an amplitude could vary quite rapidly, with energy, thereby resulting in rather large time delays, hundreds or thousands of attoseconds. These effects were found to occur both in the free and confined cases. However, owing to the sensitivity of the amplitudes near the Cooper-like minima, the large excursion of the time delay were in opposite directions in the free and confined atoms, in some cases.

A purely relativistic effect was found in the $4d_{5/2,5/2}^-$ amplitude. The time delay for free Xe, in this case, decreases monotonically in contrast to the case for Xe@C_{60} where huge excursions in the delay were exhibited, greater than 1000 as, at two different energies, very much larger than could be expected due to confinement resonances. This behavior was traced to the interference between the $4d_{5/2} \rightarrow \epsilon f_{5/2}$ and $4d_{5/2} \rightarrow \epsilon f_{7/2}$ transitions, which are different only owing to relativistic interactions. The interference generated several Cooper-like minima. As a result, the Wigner time delay exhibited huge positive and negative values in the energy region of these minima. It is, thus, evident that relativistic interactions can induce interferences, which result in large physical effects. Time-delay measurements in coincidence with spin polarization of the photoelectron and alignment or orientation of the residual ion (to determine the m quantum number of the initial state) are, however, beyond current experimental capabilities. Nevertheless, the present results should stimulate research along these lines.

Taking the weighted averages of the amplitudes, the effects of these Cooper-like minima were found to be largely gone because, by their very nature, in the vicinity of the minima, the magnitude of the amplitudes were small. Thus, they do not contribute much to the averages. Nevertheless, the results showed significant qualitative and quantitative differences between the $4d_{3/2}$ and $4d_{5/2}$ cases for both free and confined Xe, thereby indicating that relativistic effects are of importance, even away from the Cooper-like minima. It was also demonstrated that measurements of the difference in time delays between free and confined atoms should be most revealing.

[1] P. M. Paul, E. Toma, P. Breger, G. Mullot, F. Augé, P. Balcou, H. Muller, and P. Agostini, Science **292**, 1689 (2001).

[2] A. Baltuška, T. Udem, M. Uiberacker, M. Hentschel, E. Goulielmakis, C. Gohle, R. Holzwarth, V. Yakovlev, A. Scrinzi and T. Hänsch and F. Krausz, Nature (London) **421**, 611 (2003).

[3] S. A. Aseyev, Y. Ni, L. J. Frasinski, H. G. Muller, and M. J. J. Vrakking, Phys. Rev. Lett. **91**, 223902 (2003).

[4] M. Uiberacker, T. Uphues, M. Schultze, A. J. Verhoef, V. Yakovlev, M. F. Kling, J. Rauschenberger, N. M. Kabachnik, H. Schröder and M. Lezius, K. L. Kompa, H.-G. Muller, M. J. J. Vrakking, S. Hendel, U. Kleineberg, U. Heinzmann, M. Drescher, and F. Krausz, Nature (London) **446**, 627 (2007).

[5] N. G. Kelkar and M. Nowakowski, Phys. Rev. A **78**, 012709 (2008).

[6] F. Krausz and M. Ivanov, Rev. Mod. Phys. **81**, 163 (2009).

[7] M. Schultze, M. Fieß, N. Karpowicz, J. Gagnon, M. Korbman, M. Hofstetter, S. Neppl, A. L. Cavalieri, Y. Komninos, T. Mercouris, C. A. Nicolaides, R. Pazourek, S. Nagele, J. Feist, J. Burgdörfer, A. M. Azzeer, R. Ernstorfer, R. Kienberger, U. Kleineberg, E. Goulielmakis, F. Krausz, and V. S. Yakovlev, Science **328**, 1658 (2010).

[8] V. S. Yakovlev, J. Gagnon, N. Karpowicz, and F. Krausz, Phys. Rev. Lett. **105**, 073001 (2010).

[9] K. Klünder, J. M. Dahlström, M. Gisselbrecht, T. Fordell, M. Swoboda, D. Guénot, P. Johnsson, J. Caillat, J. Mauritsson, A. Maquet, R. Taïeb, and A. L'Huillier, Phys. Rev. Lett. **106**, 143002 (2011).

[10] A. Kheifets, I. Ivanov, and I. Bray, J. Phys. B **44**, 101003 (2011).

[11] I. A. Ivanov and A. S. Kheifets, Phys. Rev. A **85**, 013406 (2012).

[12] I. A. Ivanov, A. S. Kheifets, and V. V. Serov, Phys. Rev. A **86**, 063422 (2012).

[13] S. Neppl, R. Ernstorfer, E. M. Bothschafter, A. L. Cavalieri, D. Menzel, J. V. Barth, F. Krausz, R. Kienberger, and P. Feulner, Phys. Rev. Lett. **109**, 087401 (2012).

[14] R. Pazourek, S. Nagele, and J. Burgdörfer, Faraday Disc. **163**, 353 (2013).

[15] G. Dixit, H. S. Chakraborty, and M. E.-A. Madjet, Phys. Rev. Lett. **111**, 203003 (2013).

[16] R. Pazourek, S. Nagele, and J. Burgdörfer, Rev. Mod. Phys. **87**, 765 (2015).

[17] E. P. Wigner, Phys. Rev. **98**, 145 (1955).

[18] C. A. de Carvalho and H. M. Nussenzveig, Phys. Rep. **364**, 83 (2002).

[19] F. T. Smith, Phys. Rev. **118**, 349 (1960).

[20] C. Ju, D. Suter, and J. Du, Phys. Rev. A **75**, 012318 (2007).

[21] V. K. Dolmatov, A. S. Baltenkov, J.-P. Connerade, and S. T. Manson, Rad. Phys. Chem. **70**, 417 (2004), and references therein.

[22] V. K. Dolmatov, Adv. Quantum Chem. **58**, 13 (2009), and references therein.

[23] M. E. Madjet, T. Renger, D. E. Hopper, M. A. McCune, H. S. Chakraborty, J.-M. Rost, and S. T. Manson, Phys. Rev. A **81**, 013202 (2010).

[24] A. Potter, M. A. McCune, R. De, M. E. Madjet, and H. S. Chakraborty, Phys. Rev. A **82**, 033201 (2010).

[25] J. N. Maser, M. H. Javani, R. De, M. E. Madjet, H. S. Chakraborty, and S. T. Manson, Phys. Rev. A **86**, 053201 (2012).

[26] M. H. Javani, H. S. Chakraborty, and S. T. Manson, Phys. Rev. A **89**, 053402 (2014).

[27] A. Rüdel, R. Hentges, U. Becker, H. S. Chakraborty, M. E. Madjet, and Jan M. Rost, Phys. Rev. Lett. **89**, 125503 (2002).

[28] P. C. Deshmukh, A. Mandal, S. Saha, A. S. Kheifets, V. K. Dolmatov, and S. T. Manson, Phys. Rev. A **89**, 053424 (2014).

[29] J. Wätzel, A. S. Moskalenko, Y. Pavlyukh, and J. Berakdar, J. Phys. B **48**, 025602 (2015).

[30] A. Kheifets, A. Mandal, P. C. Deshmukh, V. K. Dolmatov, D. A. Keating, and S. T. Manson, Phys. Rev. A **94**, 013423 (2016).

[31] R. A. Phaneuf, A. L. D. Kilcoyne, N. B. Aryal, K. K. Baral, D. A. Esteves-Macaluso, C. M. Thomas, J. Hellhund, R. Lomsadze, T. W. Gorczyca, C. P. Ballance, S. T. Manson, M. F. Hasoğlu, S. Schippers, and A. Müller, Phys. Rev. A **88**, 053402 (2013).

[32] W. R. Johnson and C. D. Lin, Phys. Rev. A **20**, 964 (1979).

[33] W. Johnson, C. Lin, K. Cheng, and C. Lee, Phys. Scr. **21**, 409 (1980).

[34] D. A. Varshalovich, A. N. Moskalev, and V. K. Khersonskii, *Quantum Theory of Angular Momentum* (World Scientific, Singapore, 1988).

[35] W. Johnson and C. Lin, Phys. Rev. A **14**, 565 (1976).

[36] S. S. Kumar, T. Banerjee, P. C. Deshmukh, and S. T. Manson, Phys. Rev. A **79**, 043401 (2009).

[37] Y. B. Xu, M. Q. Tan, and U. Becker, Phys. Rev. Lett. **76**, 3538 (1996).

[38] H. R. Varma, P. C. Deshmukh, V. K. Dolmatov, and S. T. Manson, Phys. Rev. A **76**, 012711 (2007).

[39] M. Y. Amusia, A. Baltenkov, L. Chernysheva, Z. Felfli, and A. Msezane, J. Phys. B: At. Mol. Opt. Phys. **38**, L169 (2005).

[40] J. Connerade, V. Dolmatov, and S. T. Manson, J. Phys. B: At. Mol. Opt. Phys. **32**, L395 (1999).

[41] M. F. Hasoğlu, H.-L. Zhou, and S. T. Manson, Phys. Rev. A **93**, 022512 (2016).

[42] J.-P. Connerade, V. K. Dolmatov, and S. T. Manson, J. Phys. B **33**, 2279 (2000).

[43] A. S. Kheifets, S. Saha, P. C. Deshmukh, D. A. Keating, and S. T. Manson, Phys. Rev. A **92**, 063422 (2015).

[44] S. T. Manson, Phys. Rev. **182**, 97 (1969).

[45] A. Kivimäki, U. Hergenhahn, B. Kempgens, R. Hentges, M. N. Piancastelli, K. Maier, A Rüdel, J. J. Tulkki and A. M. Bradshaw, Phys. Rev. A **63**, 012716 (2000).

[46] M. Y. Amusia, L. V. Chernysheva, S. T. Manson, A. M. Msezane, and V. Radojević, Phys. Rev. Lett. **88**, 093002 (2002).

[47] U. Fano, Phys. Rev. **124**, 1866 (1961).

[48] J. M. Dahlström, D. Guénot, K. Klunder, M. Gisselbrecht, J. Mauritsson, A. L'Huillier, A. Maquet, and R. Taïeb, Chem. Phys. **414**, 53 (2013).

[49] J. M. Dahlström and E. Lindroth, J. Phys. B **47**, 124012 (2014); **49**, 209501 (2016).

[50] S. Heuser, Á. Jiménez-Galán, C. Cirelli, C. Marante, M. Sabbar, R. Boge, M. Lucchini, L. Gallmann, I. Ivanov, A. S. Kheifets, J. M. Dahlström, E. Lindroth, L. Argenti, F. Martín, and U. Keller, Phys. Rev. A **94**, 063409 (2016).

[51] I. A. Ivanov and A. S. Kheifets, Phys. Rev. A **96**, 013408 (2017).